

Slow photoelectron velocity-map imaging spectroscopy of the vinoxide anion

Tara I. Yacovitch,¹ Etienne Garand,¹ and Daniel M. Neumark^{1,2,a)}

¹Department of Chemistry, University of California, Berkeley, California 94720, USA

²Chemical Sciences Division, Lawrence Berkeley National Laboratory, Berkeley, California 94720, USA

(Received 24 April 2009; accepted 30 May 2009; published online 26 June 2009)

High resolution photoelectron spectra of the vinoxide anion are obtained by slow electron velocity-map imaging. Transitions between the anion \tilde{X}^1A' ground electronic state and the radical \tilde{X}^2A'' and \tilde{A}^2A' states are observed. This experiment yields a precise value of 1.8250 ± 0.0012 eV for the adiabatic electron affinity and 0.996 ± 0.003 eV for the $\tilde{A}-\tilde{X}$ term energy of the vinoxyl radical. Franck–Condon simulations of the $\tilde{X}^2A'' \leftarrow \tilde{X}^1A'$ transition are performed at varying levels of approximation. Full treatment with Duschinsky rotation is necessary to reproduce experimental results. Comparison of the experimental and simulated spectra leads to the assignment of previously unresolved transitions, notably between levels of a'' symmetry. © 2009 American Institute of Physics. [DOI: 10.1063/1.3157208]

I. INTRODUCTION

The vinoxyl radical, C_2H_3O (Fig. 1), is an important intermediate and primary product in combustion chemistry, including the $O+C_2H_4$, $OH+C_2H_2$, and $O_2+C_2H_3$ reactions.^{1–5} This species also displays complex photodissociation behavior involving conical intersections among its various low-lying electronic states^{6–9} and serves as a model system for understanding nonadiabatic effects driven by conical intersections. Experimental characterization of the spectroscopy and energetics of these low-lying states is thus crucial in order to gain a deeper understanding of vinoxyl chemistry and photochemistry. The corresponding vinoxide anion, $C_2H_3O^-$, is also of interest as it is the simplest enolate, a class of anions that provided the first evidence for dipole-bound excited electronic states.^{10,11} In this paper, we report high-resolution, slow electron velocity-map imaging (SEVI) spectra¹² of the vinoxide anion in order to probe subtleties of the energetics, vibrational structure, and electronic spectroscopy of C_2H_3O and $C_2H_3O^-$. We obtain improved values for the electron affinity (EA) and first excited state term energy of the vinoxyl radical. The SEVI spectra show considerably more vibrational structure than previous anion photoelectron spectra,^{13–15} leading to new assignments of vibrational modes in the anion and neutral.

A large body of experimental and theoretical literature exists for the vinoxyl radical. Theoretically determined energetics, structures, and frequencies for its ground and low-lying excited states can be found in many studies.^{6,14,16–21} These calculations have determined the three lowest-lying electronic states of the vinoxyl radical to be \tilde{X}^2A'' , \tilde{A}^2A' , and \tilde{B}^2A'' , all of which are planar with C_s symmetry. Electronic absorption spectra by Hunziker *et al.*¹ identified two bands, with origins at 0.99 and 3.57 eV, in reasonable agreement

with the calculated energetics for the $\tilde{A} \leftarrow \tilde{X}$ and $\tilde{B} \leftarrow \tilde{X}$ transitions,²² respectively. While the name “vinoxyl” implies an enolate-like structure, as drawn on the right of Fig. 1, this is somewhat of a misnomer for the \tilde{X} and \tilde{B} states. Geometry calculations¹⁸ and ground-state microwave data²³ show that the CO bond has more double-bond character than the CC bond. In contrast, the \tilde{A} state has significant CC double-bond character.

The microwave spectra of the vinoxyl radical and its deuterated analog provide experimental geometries for the carbon and oxygen backbone.^{23,24} Structural information is also gleaned from the extensive laser-induced fluorescence (LIF) studies of the $\tilde{B} \leftarrow \tilde{X}$ band.^{25–29} The first LIF experiments, carried out by Inoue *et al.*²⁵ and DiMauro *et al.*,²⁶ identified the main vibrations of the carbon-oxygen backbone, an additional C–H bending mode, and determined backbone geometries from rotationally resolved spectra. Brock and Rohlfling²⁷ reported LIF, dispersed fluorescence, and two-color resonant four-wave mixing spectra, identifying the nine lowest-frequency vibrational modes of the vinoxyl radical in its ground and second excited states. Photofragment yield spectroscopy of the vinoxyl radical measured by Osborn *et al.*⁶ showed that the \tilde{B} state predissociates into CH_3+CO and $H+CH_2CO$, motivating subsequent experimental^{7,29,30} and theoretical^{8,9,20,31} studies that further explored the dissociation pathways of the vinoxyl radical.

The vinoxide anion $C_2H_3O^-$, also known as acetaldehyde enolate, has an \tilde{X}^1A' ground electronic state, as determined by electronic structure calculations,^{14,32,33} with more CC double-bond character than the ground state of the radical. The dipole moment of the vinoxyl neutral core is sufficiently large to support a dipole-bound state of the anion that lies just below the detachment threshold. Excitation from the anion ground state to the dipole-bound state leads to sharp autodetaching resonances, first seen with vibrational reso-

^{a)}Author to whom correspondence should be addressed. Electronic mail: dneumark@berkeley.edu.

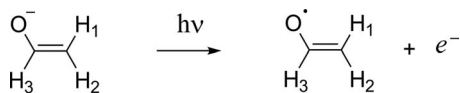


FIG. 1. Photodetachment of the vinoxide anion to produce the vinoxy radical and an electron, showing atom labels for all hydrogens.

lution by Jackson *et al.*¹⁰ and then with rotational resolution by Lineberger and co-workers.^{11,34} The CC and CO bond lengths and CCO bond angle were extracted from the rotationally resolved measurements.

Photoelectron spectra of the vinoxide anion have been reported by Ellison *et al.*¹³ and Continetti and co-workers.^{14,15} The spectrum of Ellison *et al.* yielded a value of 1.817 ± 0.023 eV for the EA of $C_2H_3O^-$, in agreement with the value obtained by Zimmerman *et al.*³⁵ via measurement of the photodetachment cross section, and showed a partially resolved vibrational progression with a 500 cm^{-1} peak spacing that was attributed to the CCO bending mode of the radical \tilde{X} state. The more recent photoelectron spectrum by Alconcel *et al.*¹⁴ at higher photon energy (3.55 eV) and better resolution exhibited transitions to the radical \tilde{X} and \tilde{A} states, yielding an EA of 1.795 ± 0.015 eV and a term energy $T_0 = 1.015 \pm 0.015$ eV for the \tilde{A} state. These spectra showed additional vibrational structure that was assigned to various vibrational modes of both neutral states with the help of electronic structure calculations and simulations. Photoelectron imaging measurements by Bowen and Continetti¹⁵ yielded photoelectron angular distributions (PADs) for detachment to the \tilde{X} and \tilde{A} states.

In this study, we present high-resolution photoelectron spectra of the vinoxide anion obtained by SEVI spectroscopy. Franck–Condon (FC) simulations are performed for the anion-to-radical ground-state transition. The SEVI spectra not only provide improved energetics for the EA and first term energy of the vinoxy radical but also resolve many vibrational features in the \tilde{X}^2A'' and \tilde{A}^2A' states that were not seen in previous photoelectron spectra. Specifically, we identify combination bands involving the low-frequency out-of-plane bending modes, leading to new assignments of these modes in the negative ion, and we observe several vibrations in the \tilde{A}^2A' state for the first time. In addition, comparison of the SEVI spectra with simulations shows clear evidence for Duschinsky rotation³⁶ between the anion and neutral normal modes, thereby probing how the nature of the vibrational levels differs in the anion and neutral.

II. EXPERIMENTAL

SEVI is a high-resolution variant of negative-ion photoelectron spectroscopy and has been described in detail previously.^{12,37} Briefly, negative ions are photodetached with a tunable laser, and the slow electrons are selectively detected using a low-voltage extraction velocity-map-imaging (VMI) setup.³⁸ By varying the detachment wavelength, a number of high-resolution scans over limited energy windows are obtained.

$C_2H_3O^-$ anions were produced from of a gas mixture comprising $\sim 1\%$ acetaldehyde in a balance of argon. The

gas mixture, at a stagnation pressure of 300 psi, was expanded into the source vacuum chamber through an Even–Lavie pulsed valve.³⁹ Anions were formed using the grid discharge source described previously.⁴⁰ These anions were mass selected⁴¹ and directed to the detachment region by a series of electrostatic lenses and pinholes. They were then photodetached between the repeller and the extraction plates of the VMI stack by the output of a Nd:YAG-pumped tunable dye laser. The photoelectron cloud formed was coaxially extracted down a 50 cm flight tube and mapped onto a detector comprising microchannel plates coupled to a phosphor screen, as is typically used in photofragment and photoelectron imaging experiments.^{42,43} Events on the screen were collected by a 1024×1024 charge-coupled device camera and sent to a computer, where they were summed, quadrant-symmetrized, smoothed, and inverse-Abel transformed.⁴⁴ Photoelectron kinetic energy spectra were obtained via angular integration of the transformed images. In each SEVI image, better energy resolution is obtained for slower electrons. Hence, by varying the laser wavelength, a series of spectra is obtained in which different transitions are well-resolved. SEVI spectra are plotted with respect to electron binding energy (eBE), defined as the difference between the photodetachment photon energy and the measured electron kinetic energy.

The apparatus was calibrated by acquiring SEVI images of atomic S^- and Cl^- at several different photon energies. With the 350 V VMI repeller voltage used in this study, a Gaussian peak width ($w = 2\sigma$) of 4.3 cm^{-1} was obtained for a chloride peak at 32.3 cm^{-1} above threshold. Linewidths in the spectra presented here are limited by unresolved rotational structure, and since the origin of an unresolved rotational profile may not be aligned with the observed peak maximum, we report error bars of one Gaussian standard deviation ($\frac{1}{2}w = \sigma$) for all energy determinations.

SEVI also provides information on the photoelectron angular distribution. For one-photon detachment, the PAD is given by^{45,46}

$$\frac{d\sigma}{d\Omega} = \frac{\sigma_{\text{tot}}}{4\pi} \left(1 + \beta \left(\frac{3}{2} \cos^2(\theta) - \frac{1}{2} \right) \right), \quad (1)$$

where θ is the angle between the direction of the photoelectron ejection and the polarization vector of the incident photon. The anisotropy parameter β is sensitive to the shape and symmetry of the molecular orbital from which detachment occurs. It lies between 2 and -1 , yielding $\cos^2 \theta$ and $\sin^2 \theta$ limiting PADs, respectively.

III. RESULTS

SEVI spectra of the vinoxide $\tilde{X}^2A'' \leftarrow \tilde{X}^1A'$ and $\tilde{A}^2A' \leftarrow \tilde{X}^1A'$ photodetachment transitions are presented in Figs. 2 and 3, respectively. Peak positions and assignments are summarized in Table I. The anisotropy parameter β is negative for all transitions in Fig. 2 and positive for all transitions in Fig. 3, consistent with earlier results.¹⁵ Though only a few traces are shown for clarity, several scans were taken at progressively lower photon energies in order to achieve high resolution for all peaks. Peak positions are taken from the

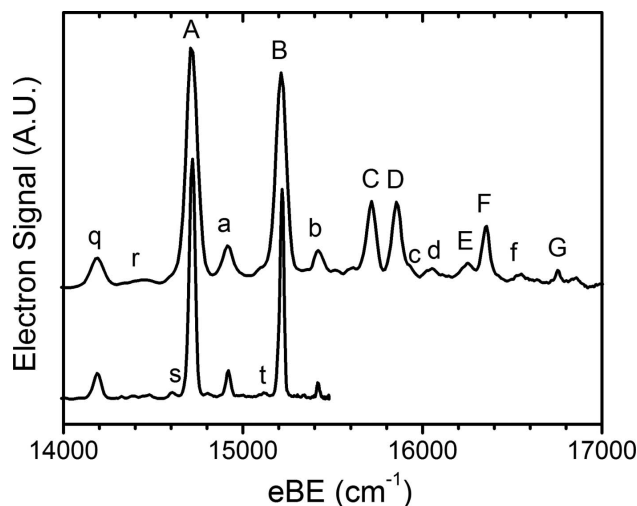


FIG. 2. SEVI spectra of vinoxide, $C_2H_2O^-$, showing transitions to the radical \tilde{X}^2A'' state and covering an eBE range of 14 000–17 000 cm^{-1} . The top trace is an average of three scans taken near a photon energy of 15 492 cm^{-1} ; the bottom is an average of two scans near a photon energy of 17 239 cm^{-1} .

highest resolution scan taken for that peak. Near threshold, peaks as narrow as $w=19$ cm^{-1} were observed; as discussed above, this resolution limit reflects unresolved rotational structure.

In Fig. 2, the band origin A occurs at $14\,719 \pm 9$ cm^{-1} , and peaks A–C constitute a clear progression of peaks spaced by 498 cm^{-1} . Peaks D, E, F, and G appear at 1137, 1528, 1634, and 2036 cm^{-1} from peak A, respectively. Five weaker peaks are also present, each of which lies around 200 cm^{-1} higher than a larger peak. These are labeled a, b, c, d, and f. The four remaining peaks are labeled q, r, s, and t. As discussed in Sec. V, the upper case peaks are assigned to transitions from the anion vibrational ground state, while the lower case peaks are hot band or sequence band transitions.

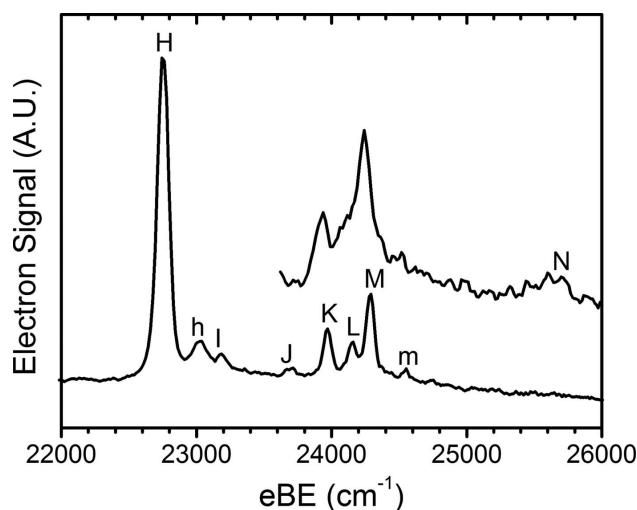


FIG. 3. SEVI spectra of vinoxide, $C_2H_2O^-$, showing transitions to the radical \tilde{A}^2A' state and covering an eBE range of 22 000–26 000 cm^{-1} . The top trace is an average of two scans taken near a photon energy of 26 525 cm^{-1} (a high enough energy that the origin peak falls outside the detector radius). The bottom trace is an average of three scans near a photon energy of 28 370 cm^{-1} .

TABLE I. Experimental peak positions, shifts from the origin bands, and assignments.

Label ^a	Position (cm^{-1})	Shift (cm^{-1})	Assignment ^b
Vinoxy \tilde{X}^2A'' state			
q	14 195	−524	9_0^0
r	14 435	−284	12_1^1
s	14 609	−110	$10_1^1?$
A	14 719	0	0-0
a	14 918	199	11_1^1
t	15 112	392	$9_0^1 10_1^1?$
B	15 217	498	9_0^1
b	15 419	699	$9_0^1 11_1^1$
C	15 716	997	9_0^2
D	15 856	1137	7_0^1
c	15 925	1206	$9_0^2 11_1^1$
d	16 049	1330	$7_0^1 11_1^1$
E	16 247	1528	4_0^1 and 9_0^3
F	16 353	1634	$9_0^1 7_0^1$
f	16 542	1823	$9_0^1 7_0^1 11_1^1$
G	16 755	2036	$9_0^2 7_0^1$
Vinoxy \tilde{A}^2A' state			
H	22 751	0	0-0
h	23 010	259	$11_1^1?$
I	23 175	424	9_0^1
J	23 677	925	8_0^1
K	23 970	1218	6_0^1
L	24 155	1404	5_0^1
M	24 285	1533	4_0^1
m	24 548	1797	$4_0^1 11_1^1?$
N	25 706	2955	$4_0^1 5_0^1?$

^aLabels refer to Figs. 2 and 3.

^bNormal modes are described in Table III.

The SEVI spectrum shows many more features than either of the previously reported photoelectron spectra of this band,^{13,14} both of which were dominated by a partially resolved progression of peaks spaced by around 500 cm^{-1} . While we observe such a progression as well (peaks A–C), the SEVI spectrum clearly shows contributions from multiple vibrational modes.

The spectra in Fig. 3 are dominated by the band origin, peak H, at $22\,751 \pm 20$ cm^{-1} . A grouping of peaks (K, L, and M) appear at 1218, 1403, and 1533 cm^{-1} from peak H, with a second grouping of poorly resolved, low-intensity peaks (N) appearing at binding energies at around 25 600 cm^{-1} . Two low-intensity transitions, h and I, appear a few hundred wavenumbers from peak H, and two other low energy transitions are resolvable at 925 and 1796 cm^{-1} from peak H (peaks J and m). Again, many more peaks are resolved here than in the previous photoelectron spectrum of this band.¹⁴

IV. ANALYSIS

A. Electronic structure calculations

Geometry optimizations and frequency calculations were performed on the ground states of the vinoxide radical and vinoxide anion in order to obtain normal mode displacements, geometries, and frequencies for both states at a consistent level of theory. Density functional theory was chosen

TABLE II. Calculated geometries for the vinoxide and vinoxyl ground states using density functional theory, the B3LYP functional, and the 6-311++G** basis set. (Atom labels refer to Fig. 1.)

	Vinoxide \tilde{X}^1A'	Vinoxyl \tilde{X}^2A'
Bond lengths (Å)		
CC	1.384	1.424
CO	1.267	1.235
CH(1)	1.088	1.084
CH(2)	1.087	1.084
CH(3)	1.127	1.105
Bond angles (deg)		
OCC	130.4	123.1
CCH(3)	112.8	116.9
CCH(1)	121.4	119.4
CCH(2)	119.9	121.0

because it balances acceptable accuracy with a low computational load. The B3LYP functional was used along with Pople-style basis sets. A number of calculations were performed, and the 6-311++G** basis set performed most reasonably. It is used in all of the results given here. All frequencies were scaled by a factor of 0.9679 as is standard for B3LYP calculations with Pople-style basis sets.⁴⁷ The GAUSSIAN 03 suite of programs⁴⁸ was used throughout.

Our calculated geometries for the vinoxyl and vinoxide ground states are shown in Table II. These results are in good agreement with calculations performed at higher levels of theory.^{14,18} The backbone geometries also compare well to the experimental values derived from studying dipole-bound states of the anion¹¹ and rotational structure of the radical ground state.²³ The most striking difference in the calculated

geometries between the anion and radical ground states is the approximately 7° difference in CCO bond angles, leading us to expect a photoelectron spectrum dominated by a progression of the CCO bending mode.

Scaled frequencies for the anion and radical \tilde{X} states and their normal mode descriptions appear in Table III. Previous experimental and theoretical results for all states are also shown for comparison. The anion and radical \tilde{X} state vibrational modes are similar and within each symmetry (a' or a'') are ordered according to their value in the radical \tilde{X} state; using such a scheme, the anion ν_{11} frequency is lower than the ν_{12} frequency. The \tilde{A} state normal modes, which differ in character from the modes in either the anion or neutral \tilde{X} states, are numbered according to the scheme of Alconcel *et al.*¹⁴

With the exception of the three CH stretching modes in the anion, ν_1 , ν_2 , and ν_3 , which exhibit no observable activity in the anion photoelectron spectrum,^{13,14} all other a' frequencies agree to within 50 cm⁻¹ of previous calculations (Table III). Among the calculated a'' modes, the ν_{10} and ν_{11} frequencies differ most from previous experiment and simulations. As discussed in Sec. V, these inconsistencies will not affect the experimental frequency determinations.

B. FC simulations

FC simulations were performed on the $\tilde{X}^2A'' \leftarrow \tilde{X}^1A'$ band using frequencies and geometries from the electronic structure calculations. Line intensities are proportional to FC factors for the overlap between the anion and neutral vibrational wavefunctions, ψ_v^i and ψ_v^f , respectively,

TABLE III. Normal modes and scaled vibrational frequencies (cm⁻¹) of the vinoxide anion and vinoxyl radicals.

Mode	Description	Sym.	Vinoxide \tilde{X}^1A'				Vinoxyl \tilde{X}^2A''				Mode	Description ^b	Sym.	Vinoxyl \tilde{A}^2A'		
			Calc. ^a	Calc. ^b	Expt. ^a	Expt. ^c	Calc. ^a	Calc. ^b	Expt. ^a	Expt. ^d				Calc. ^b	Expt. ^a	Expt. ^b
ν_1	CH ₂ asymmetric stretch	a'	3068	3013			3148	3110			ν_1	CH asymmetric stretch	a'	3095		
ν_2	CH ₂ symmetric stretch	a'	2986	2853			3037	3004			ν_2	CH stretch	a'	3025		
ν_3	CH(3) stretch	a'	2585	2660			2849	2890			ν_3	CH symmetric stretch	a'	3005		
ν_4	CO stretch	a'	1550	1568			1496	1525	1528	1543	ν_4	CC stretch	a'	1590	1533	1580
ν_5	CH ₂ bend (scissors)	a'	1396	1425			1423	1441		1486	ν_5	CH ₂ scissors	a'	1403	1403	1350
ν_6	HCO bend	a'	1308	1340			1350	1373		1366	ν_6	OCH bend	a'	1258	1218	
ν_7	CC stretch	a'	1182	1179			1120	1101	1137	1143	ν_7	CO stretch	a'	1083		
ν_8	CH ₂ rock	a'	960	976			946	934		957	ν_8	CH ₂ rock	a'	929	925	
ν_9	CCO bend	a'	514	519	524	525	490	489	498	500	ν_9	CCO bend	a'	441	423	460
ν_{10}	CH(3) out of plane wag	a''	939	966	813 ^c		943	892		703	ν_{10}	Out-of-plane mode	a''	847		
ν_{11}	All CH wag	a''	469	420	358 ^c		734	599		557	ν_{11}	Out-of-plane mode	a''	627	617 ^c	
ν_{12}	CH ₂ twist	a''	670	643	688 ^c	375	429	406		404	ν_{12}	Out-of-plane mode	a''	180		

^aThis work.

^bReference 14.

^cReference 11.

^dReference 27.

^eAnion \tilde{X} and radical \tilde{A} state frequencies are deduced from radical \tilde{X} state frequencies in Ref. 27 and experimentally observed sequence band transitions of type ν_1^j . See Sec. V of the text.

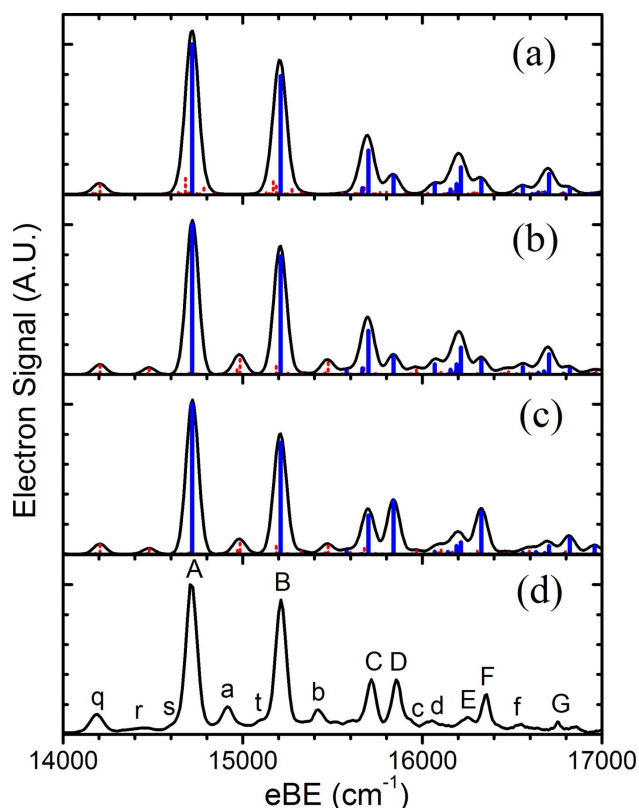


FIG. 4. (Color online) Comparison of simulated and experimental spectra for the \tilde{X}^2A' state of vinoxide. Panel (a) shows simulated results using the parallel mode approximation with no mode matching. Panel (b) shows simulated results using the parallel mode approximation and manually matching normal modes (see text). Panel (c) shows results from a FC simulation using Duschinsky rotation for all modes. Panel (d) shows the overview experimental spectrum from Fig. 2. In panels (a)–(c), the solid (blue) line spectra show transitions originating from the anion ground state. The dotted (red) line spectra show transitions originating from vibrationally excited anion states populated at 300 K. Gaussian convolutions of the full 300 K line spectra at $w=0.0085$ eV are also shown.

$$FC = \left| \int \psi_{\nu'}^* \cdot \psi_{\nu} d\tau \right|^2. \quad (2)$$

The Born–Oppenheimer principle is assumed, as well as a constant electronic transition moment. The initial (Q) and final (Q') normal coordinates are related by the Duschinsky transformation,³⁶

$$Q = JQ' + K. \quad (3)$$

Here, J is the Duschinsky rotation matrix, which represents the mixing of normal modes. K is the normal coordinate displacement vector that expresses the difference between the neutral and anion equilibrium geometries in terms of the anion normal coordinates. One can often invoke the parallel mode approximation, in which the J matrix is assumed to be the unit matrix when simulating photoelectron spectra. This approximation assumes that the active normal modes have the same form in the anion and neutral. However, as shown below, the parallel mode approximation is inadequate for simulating the vinoxide SEVI spectrum.

Simulations of the $\tilde{X}^2A' \leftarrow \tilde{X}^1A'$ transition appear in order of increasing sophistication in panels (a)–(c) of Fig. 4. Panel (d) shows an experimental SEVI overview spectrum.

All simulations were performed with the FCGAUSS03 (Ref. 49) and PESCAL (Ref. 50) programs at Boltzmann temperatures of 0 and 300 K. The Sharp and Rosenstock⁵¹ method with corrections by Chen⁵² was used to calculate FC intensities.

Panel (a) in Fig. 4 shows the usual parallel mode approximation, in which the normal modes of each symmetry type are ordered according to decreasing frequency, with the lowest-frequency mode numbered the highest. In this treatment, peaks r, a, and b seen in the experimental spectrum are missing, and the relative intensities of peaks C–F are poorly reproduced. One problem with this level of approximation is readily apparent from Table III, which shows that the lowest-frequency a'' modes in the anion and neutral, both of which are assumed to be the ν_{12} mode in panel (a), correspond to different vibrational motions, namely, CH out-of-plane wagging and CH₂ twisting, respectively. The analogous problem arises with the second lowest-frequency a'' modes. This issue can be addressed to some extent by using the numbering scheme in Table III, in which we have manually matched similar normal modes in the anion and neutral, so that the ν_{11} and ν_{12} modes correspond to the same type of vibration. In the resulting simulation, shown in panel (b), peaks r, a, and b are now apparent, indicating that they correspond to transitions involving the ν_{11} and ν_{12} modes, but the relative intensities of the four peaks C–F are unchanged.

Upon inclusion of Duschinsky rotation in panel (c) of Fig. 4, the simulated intensities match the experimental results much better. The J matrix is block diagonal; only modes of the same symmetry are mixed. All a'' modes are strongly mixed (eliminating the need to manually reorder modes), and a few a' modes are also moderately mixed, notably ν_4 and ν_7 . The good overall agreement between the simulated and experimental spectra without adjusting the calculated frequencies or geometries facilitates assignment of nearly all spectral features, as discussed in Sec. V.

V. DISCUSSION

Peak positions and assignments are reported in Table I. Throughout Sec. V, results from the full FC simulations [panel (c) in Fig. 4] were used to support assignments in the $\tilde{X}^2A' \leftarrow \tilde{X}^1A'$ band. The FC results of Alconcel *et al.*¹⁴ for the $\tilde{A}^2A' \leftarrow \tilde{X}^1A'$ transition also provide a basis for assigning many of the \tilde{A} state peaks, although they included only six of the nine totally symmetric normal modes in their simulations and excluded all a'' vibrations. The notation ν_n^m is used throughout, where ν refers to the normal mode of either the \tilde{X} or \tilde{A} state of the radical, based on the numbering scheme in Table III.

A. Energetics

This study provides improved values for the EA and \tilde{A} state term energy (T_0) of the vinoxide radical. Peak A at $14\,719 \pm 9$ cm⁻¹ in Fig. 2 is the origin of the $\tilde{X}^2A' \leftarrow \tilde{X}^1A'$ transition and peak H at $22\,751 \pm 20$ cm⁻¹ in Fig. 3 is the origin of the $\tilde{A}^2A' \leftarrow \tilde{X}^1A'$ transition. These peak positions yield EA = 1.8250 ± 0.0012 eV and T_0

$=0.996 \pm 0.003$ eV. Comparison of our results to the previously reported photoelectron spectra at lower resolution shows that our EA is well within the error bars of the value of 1.817 ± 0.023 eV reported by Ellison *et al.*,¹³ but just outside the error bars of the more recent value reported by Alconcel *et al.*,¹⁴ 1.795 ± 0.015 eV. Similarly, our T_0 is just beyond the value of 1.015 ± 0.015 eV reported by Alconcel *et al.*¹⁴ but compares favorably to the previously reported theoretical values.¹⁸ It is possible that in Ref. 14, the presence of unresolved hot bands (like peak q in Fig. 2) biased the determination of EA toward lower energy, simultaneously increasing the value of T_0 extracted from the same spectrum.

B. Vinyoxy \tilde{X} state

Aside from the band origin, peak A, the most prominent features in the $\tilde{X}^2A'' \leftarrow \tilde{X}^1A'$ spectra (Fig. 2) involve bending and stretching modes of the CCO backbone. Peaks B, C, and E are assigned to a progression in the ν_9 CCO bending mode with spacings of 498 cm^{-1} for A-B and B-C and a C-E spacing of 531 cm^{-1} . FC simulations [panel (c) in Fig. 4] suggest that peak E at 1528 cm^{-1} also includes a contribution from the 4_0^1 transition of the CO stretching mode, observed at a frequency of 1543 cm^{-1} in LIF experiments;²⁷ this is why the C-E spacing differs from other members of the progression. Peak D, at 1137 cm^{-1} from the origin, is assigned to the 7_0^1 transition in the ν_7 CC stretching mode. (We and others¹⁴ find that Brock's descriptions of modes ν_7 and ν_8 are interchanged.) The ν_7 fundamental in vinyoxy was measured by LIF as 1143 cm^{-1} .²⁷ Peak F is a combination band of the ν_7 and ν_9 modes: $9_0^1 7_0^1$.

Peaks E (9_0^3 and 4_0^1), D(7_0^1), and F($9_0^1 7_0^1$) have intensities that are only well-simulated upon inclusion of Duschinsky rotation [panel (c) in Fig. 4]. This is because modes ν_7 and ν_4 are mixed: In the J matrix, the CC stretching mode ν_7 has significant off-diagonal elements involving ν_4 , ν_5 , ν_6 , and ν_8 . It is not too surprising that the CC and CO stretches have very different normal mode descriptions in the anion versus the neutral; upon electron detachment, there is a large change in backbone bond lengths and bond angle relative to the rest of the molecular frame.

Peak q is assigned to a hot band of the bending mode 9_0^1 , consistent with simulation and previous photodetachment experiments.³⁴ This assignment yields an anion bending frequency of 524 cm^{-1} , in excellent agreement with the previously calculated values. Other hot bands that might be expected are ν_0^2 or ν_1^1 transitions of a'' out-of-plane normal modes (i.e., $\Delta\nu = \text{even}$), which are FC allowed in the absence of vibronic coupling. Simulations identify peak a, at 199 cm^{-1} above the band origin, as the 11_1^1 sequence band of the a'' CH wagging mode ν_{11} . Peaks b-d and f also occur at binding energies around 200 cm^{-1} higher than the major peaks B-D and F, and are thus all assigned as combination bands of those major transitions with the 11_1^1 sequence band. Precise LIF determination of the radical ν_{11} frequency at 557 cm^{-1} by Brock and Rohlfing²⁷ allows us to deduce an anion ν_{11} frequency of 358 cm^{-1} . This value is smaller than our calculated predictions (Table III) by about 60 cm^{-1} .

Transitions analogous to peaks a and b were observed in studies by Mead *et al.*¹¹ but were assigned to ν_0^2 transitions of the torsional mode (ν_{12} in this paper). This assignment yielded a ground-state radical torsional frequency of 100 cm^{-1} , more than 300 cm^{-1} smaller than both the calculated and LIF experimental torsional frequencies (Table III), so we believe our assignment is preferable.

The weak peak r, at a binding energy of 284 cm^{-1} lower than the origin transition, is assigned to a sequence band of a torsional vibration about the CC bond, 12_1^1 . This assignment is based on our FC calculations and previous detachment data from Mead *et al.* who identified a similar transition at 278 cm^{-1} below the origin. The frequency of the ν_{12} CC bond torsion is calculated to be around 260 cm^{-1} lower in the radical than in the anion (Table III), in agreement with the difference in CC double-bond character. Again, no direct determination of the ν_{12} frequency is possible, but based on the radical frequency of 404 cm^{-1} as determined by LIF,²⁷ the anion ν_{12} frequency is 688 cm^{-1} . This SEVI result is much closer to the predicted frequencies than the value of 375 cm^{-1} reported by Mead *et al.* (Table III), which was based on their assumption that the neutral ν_{12} frequency was 100 cm^{-1} .

Peaks s and t occur at binding energies around 100 cm^{-1} lower than peaks A and B. No features in the simulations in Fig. 4 occur at the correct position. Assuming a hot band transition of type ν_1^1 , the frequency in the anion must be 100 cm^{-1} higher than in the radical. No modes in our calculations correspond to this difference, but in the CASSCF frequency calculations by Alconcel *et al.*,¹⁴ modes ν_7 and ν_{10} differ by 78 and 74 cm^{-1} , respectively. Tentative assignments of these hot bands are 7_1^1 or 10_1^1 for peak s and $7_1^1 9_0^1$ or $10_1^1 9_0^1$ for peak t. One might favor sequence bands of ν_{10} , an out-of-plane wagging mode of the α -hydrogen H(3), since its frequency in the anion is slightly lower than that of the ν_7 mode, resulting in a higher population at a given temperature. The discharge source typically yields fairly cold ions, of the order of 70 K, but simulations at this temperature did not reproduce the spectrum as well as at 300 K, the value assumed in panel (c).

The SEVI spectra for the $\tilde{X}^1A' \leftarrow \tilde{X}^2A''$ transition yield new assignments for sequence bands involving the out-of-plane modes, leading to the determination of the ν_{10} , ν_{11} and ν_{12} frequencies in the anion. The \tilde{X} state spectrum is also a clear example of a case where Duschinsky rotation has a large effect on the simulated spectrum; the mixing of normal modes between anion and neutral is essential to describing transitions between states where geometries and CC and CO double-bond character are significantly different.

C. Vinyoxy \tilde{A} state

In accordance with previous photoelectron experiments,¹⁴ peak H at $22\,751$ cm^{-1} in Fig. 3 is assigned to the origin of the $\tilde{A}^2A' \leftarrow \tilde{X}^2A'$ band. Other features can be assigned using the simulated spectrum of Alconcel *et al.*¹⁴ The first major cluster of peaks after the origin transition appears at around $24\,500$ cm^{-1} . The peaks in this cluster, labeled K, L, and M, are assigned to the 6_0^1 , 5_0^1 , and 4_0^1 tran-

sitions involving the ν_6 OCH bend, the ν_5 CH₂ scissors and the ν_4 CC stretch, respectively. Our spectrum represents the first experimental observation of the OCH bending mode at 1218 cm⁻¹, in good agreement with the calculated frequency of 1258 cm⁻¹. The experimental frequencies for the CH₂ scissors, 1403 cm⁻¹, and the CC stretch, 1533 cm⁻¹, are also in good agreement with theory but differ slightly from lower resolution experiments (see Table III) where the cluster of peaks at binding energies of 24 500 cm⁻¹ was not resolved.¹⁴ A second grouping of peaks appears at around 25 700 cm⁻¹ is labeled N in Fig. 3. The intensity this far from threshold is too low to make definitive peak assignments, but the grouping likely contains peaks of type ν_0^2 for the ν_6 , ν_5 , and ν_4 vibrations, or combinations thereof.

The small peak I at 423 cm⁻¹ from the H origin peak is assigned to the CCO bending mode, in good agreement with the previously calculated frequency of 441 cm⁻¹ (Table III). Its experimental intensity is much lower than simulated,¹⁴ indicating that the \tilde{A} state CCO bond angle may be closer to the anion CCO bond angle than calculated. The next feature, peak J at 925 cm⁻¹, corresponds well to the predicted position for the CH₂ rocking mode ν_8 at 929 cm⁻¹. This transition was not observed at lower resolution,¹⁴ but it is now evident that it was present as a shoulder to the neighboring intense peak, and that the previous simulation overestimated its intensity.

Two low-intensity transitions, h and m, appear around 260 cm⁻¹ above the intense transitions H and M. Analogous to the assignments in the $\tilde{X}^2A' \leftarrow \tilde{X}^1A'$ band, these small features are assigned to sequence band transitions of type ν_1^1 between out-of-plane bending modes. A value of 617 cm⁻¹ for the ν_{11} bending mode in the excited \tilde{A} state radical can be deduced based on the SEVI experimental value for the frequency of the ν_{11} mode in the anion, which was itself extrapolated from the LIF value for this transition in the \tilde{X} state radical.²⁷ This value agrees well with frequency calculations, which identify an out-of-plane mode at 627 cm⁻¹ (Table III).

The SEVI spectra for the $\tilde{X}^2A' \leftarrow \tilde{X}^1A'$ band resolve a number of previously unobserved peaks. The low-intensity 9_0^1 transition indicates that anion and excited state radical have similar CCO bond angles, in contrast to the $\tilde{X}^2A' \leftarrow \tilde{X}^1A'$ band. The ν_6 OCH bending mode and ν_8 CH₂ rocking modes are identified for the first time along with sequence bands between out-of-plane bending modes, which yield an experimental frequency of 617 cm⁻¹ for the \tilde{A} state ν_{11} mode.

VI. CONCLUSIONS

SEVI is used to obtain high-resolution photoelectron spectra of the vinoxide anion, C₂H₃O⁻. Previously unresolved transitions to the \tilde{X} and \tilde{A} states of the vinoxyl radical are observed, notably sequence band transitions involving modes of a'' symmetry. Improved values are obtained for the EA of vinoxyl and the \tilde{A} - \tilde{X} term energy. Experimental assignments are aided by comparison with FC simulations and calculated frequencies, yielding new frequencies for selected

vibrational modes in the anion and in the neutral \tilde{A} state. Ground-state simulations with and without use of Duschinsky rotation reveal that the vinoxyl system is a case where inclusion of Duschinsky rotation makes a significant difference in the FC simulation and results in much improved agreement with experiment.

ACKNOWLEDGMENTS

This work was supported by the Air Force Office of Scientific Research under Grant No. F49620-03-1-0085. T.I.Y. thanks the Fonds Québécois de la Recherche sur la Nature et les Technologies (FQRNT) for a master's scholarship. E.G. thanks the National Science and Engineering Research Council of Canada (NSERC) for a postgraduate scholarship.

- ¹H. E. Hunziker, H. Knepe, and H. R. Wendt, *J. Photochem.* **17**, 377 (1981).
- ²V. Schmidt, G. Y. Zhu, K. H. Becker, and E. H. Fink, *Ber. Bunsenges. Phys. Chem.* **89**, 321 (1985).
- ³A. M. Schmoltner, P. M. Chu, R. J. Brudzynski, and Y. T. Lee, *J. Chem. Phys.* **91**, 6926 (1989).
- ⁴J. Lee and J. W. Bozzelli, *Int. J. Chem. Kinet.* **35**, 20 (2003).
- ⁵P. Casavecchia, G. Capozza, E. Segoloni, F. Leonori, N. Balucani, and G. G. Volpi, *J. Phys. Chem. A* **109**, 3527 (2005).
- ⁶D. L. Osborn, H. Choi, D. H. Mordaunt, R. T. Bise, D. M. Neumark, and C. M. Rohlfing, *J. Chem. Phys.* **106**, 3049 (1997).
- ⁷M. L. Morton, D. E. Szpunar, and L. J. Butler, *J. Chem. Phys.* **115**, 204 (2001).
- ⁸S. Matsika and D. R. Yarkony, *J. Chem. Phys.* **117**, 7198 (2002).
- ⁹K. Piechowska-Strumik, D. Lauvergnat, M. C. Bacchus-Montabonel, and M. Desouter-Lecomte, *Chem. Phys. Lett.* **425**, 16 (2006).
- ¹⁰R. L. Jackson, P. C. Hiberty, and J. I. Brauman, *J. Chem. Phys.* **74**, 3705 (1981).
- ¹¹R. D. Mead, K. R. Lykke, W. C. Lineberger, J. Marks, and J. I. Brauman, *J. Chem. Phys.* **81**, 4883 (1984).
- ¹²D. M. Neumark, *J. Phys. Chem. A* **112**, 13287 (2008).
- ¹³G. B. Ellison, P. C. Engelking, and W. C. Lineberger, *J. Phys. Chem.* **86**, 4873 (1982).
- ¹⁴L. S. Alconcel, H. J. Deyerl, V. Zengin, and R. E. Continetti, *J. Phys. Chem. A* **103**, 9190 (1999).
- ¹⁵M. S. Bowen and R. E. Continetti, *J. Phys. Chem. A* **108**, 7827 (2004).
- ¹⁶E. S. Huyser, D. Feller, W. T. Borden, and E. R. Davidson, *J. Am. Chem. Soc.* **104**, 2956 (1982).
- ¹⁷M. Yamaguchi, T. Momose, and T. Shida, *J. Chem. Phys.* **93**, 4211 (1990).
- ¹⁸P. Botschwina, *Mol. Phys.* **103**, 1441 (2005).
- ¹⁹M. Yamaguchi, S. Inomata, and N. Washida, *J. Phys. Chem. A* **110**, 12419 (2006).
- ²⁰D. I. G. Bennett, L. J. Butler, and H. J. Werner, *J. Chem. Phys.* **127**, 094309 (2007).
- ²¹R. A. Young and D. R. Yarkony, *J. Chem. Phys.* **123**, 084315 (2005).
- ²²M. Dupuis, J. J. Wendoloski, and W. A. Lester, *J. Chem. Phys.* **76**, 488 (1982).
- ²³Y. Endo, S. Shuji, and E. Hirota, *J. Chem. Phys.* **83**, 2026 (1985).
- ²⁴Y. Endo and E. Hirota, *J. Mol. Spectrosc.* **127**, 535 (1988).
- ²⁵G. Inoue, M. Okuda, and H. Akimoto, *J. Chem. Phys.* **75**, 2060 (1981).
- ²⁶L. F. DiMauro, M. Heaven, and T. A. Miller, *J. Chem. Phys.* **81**, 2339 (1984).
- ²⁷L. R. Brock and E. A. Rohlfing, *J. Chem. Phys.* **106**, 10048 (1997).
- ²⁸R. L. Wan, X. R. Chen, F. Wu, and B. R. Weiner, *Chem. Phys. Lett.* **260**, 539 (1996).
- ²⁹H. Su and R. Bersohn, *J. Chem. Phys.* **115**, 217 (2001).
- ³⁰J. L. Miller, L. R. McCunn, M. J. Krisch, L. J. Butler, and J. Shu, *J. Chem. Phys.* **121**, 1830 (2004).
- ³¹J. P. Senozian, S. J. Klippenstein, and J. A. Miller, *J. Phys. Chem. A* **110**, 5772 (2006).
- ³²R. W. Wetmore, H. F. Schaefer, P. C. Hiberty, and J. I. Brauman, *J. Am. Chem. Soc.* **102**, 5470 (1980).

- ³³D. O'Neal and J. Simons, *J. Phys. Chem.* **93**, 58 (1989).
- ³⁴A. S. Mullin, K. K. Murray, C. P. Schulz, D. M. Szaflarski, and W. C. Lineberger, *Chem. Phys.* **166**, 207 (1992).
- ³⁵A. H. Zimmerman, K. J. Reed, and J. I. Brauman, *J. Am. Chem. Soc.* **99**, 7203 (1977).
- ³⁶F. Duschinsky, *Acta Physicochim. URSS* **7**, 551 (1937).
- ³⁷A. Osterwalder, M. J. Nee, J. Zhou, and D. M. Neumark, *J. Chem. Phys.* **121**, 6317 (2004).
- ³⁸A. Eppink and D. H. Parker, *Rev. Sci. Instrum.* **68**, 3477 (1997).
- ³⁹U. Even, J. Jortner, D. Noy, N. Lavie, and C. Cossart-Magos, *J. Chem. Phys.* **112**, 8068 (2000).
- ⁴⁰E. Garand, T. I. Yacovitch, and D. M. Neumark, *J. Chem. Phys.* **130**, 064304 (2009).
- ⁴¹W. C. Wiley and I. H. McLaren, *Rev. Sci. Instrum.* **26**, 1150 (1955).
- ⁴²D. W. Chandler and P. L. Houston, *J. Chem. Phys.* **87**, 1445 (1987).
- ⁴³A. Sanov and R. Mabbs, *Int. Rev. Phys. Chem.* **27**, 53 (2008).
- ⁴⁴E. W. Hansen and P.-L. Law, *J. Opt. Soc. Am. A* **2**, 510 (1985).
- ⁴⁵J. Cooper and R. N. Zare, *J. Chem. Phys.* **48**, 942 (1968).
- ⁴⁶K. L. Reid, *Annu. Rev. Phys. Chem.* **54**, 397 (2003).
- ⁴⁷M. P. Andersson and P. Uvdal, *J. Phys. Chem. A* **109**, 2937 (2005).
- ⁴⁸M. J. Frisch, G. W. Trucks, H. B. Schlegel *et al.*, GAUSSIAN 03, Revision C. 02, Gaussian, Inc., Wallingford CT, 2004.
- ⁴⁹K. M. Ervin, FCFGAUSS03: Gaussian 03 Output Conversion Program, 2004.
- ⁵⁰K. M. Ervin, PESCAL, Fortran program, 2008.
- ⁵¹T. E. Sharp and H. M. Rosenstock, *J. Chem. Phys.* **41**, 3453 (1964).
- ⁵²P. Chen, in *Unimolecular and Bimolecular Reaction Dynamics*, edited by T. Baer, C.-Y. Ng, and I. Powis (Wiley, Chichester, 1994), p. 371.